HHS Public Access

Author manuscript

Curr Biol. Author manuscript; available in PMC 2020 December 02.

Published in final edited form as:

Curr Biol. 2019 December 02; 29(23): 4130–4138.e5. doi:10.1016/j.cub.2019.10.017.

Defined cell types in superior colliculus make distinct contributions to prey capture behavior in the mouse

Jennifer L. Hoy[1], **Hannah I. Bishop**[2], **Cristopher M. Niell**[2]

[1]Department of Biology, University of Nevada, Reno, Reno NV 89557 USA,

[2]Department of Biology and Institute of Neuroscience, University of Oregon, Eugene OR 97403 USA

Summary

The superior colliculus (SC) plays a highly conserved role in visual processing, and mediates visual orienting behaviors across species, including both overt motor orienting [1,2] and orienting of attention [3,4]. To determine the specific circuits within the superficial SC that drive orienting and approach behavior toward appetitive stimuli, we explored the role of three genetically defined cell types in mediating prey capture in mice. Chemogenetic inactivation of two classically defined cell types, the wide-field (WF) and narrow-field (NF) vertical neurons, revealed that they are involved in distinct aspects of prey capture. WF neurons were required for rapid prey detection and distant approach initiation, whereas NF neurons were required for accurate orienting during pursuit as well as approach initiation and continuity. In contrast, prey capture did not require parvalbumin-expressing (PV) neurons that have previously been implicated in fear responses. The visual coding and projection targets of WF and NF cells were consistent with their roles in prey detection versus pursuit, respectively. Thus, our studies link specific neural circuit connectivity and function with stimulus detection and orienting behavior, providing insight into visuomotor and attentional mechanisms mediated by superior colliculus.

Graphical Abstract

Correspondence : Jennifer Hoy (jhoy@unr.edu), Cristopher Niell (cniell@uoregon.edu).

Author Contributions

Conceptualization, J.L.H. and C.M.N.; Methodology and Formal Analysis J.L.H. and C.M.N.; Software, C.M.N and J.L.H; Investigation, J.L.H. and H.I.B ; Visualization, J.L.H. and C.M.N.; Writing – Original Draft, J.L.H.; Writing – Review & Editing, J.L.H., C.M.N., and H.I.B.; Resources, C.M.N.

Lead Contact : Cristopher Niell (cniell@uoregon.edu)

Declaration of Interests

The authors declare no competing interests.

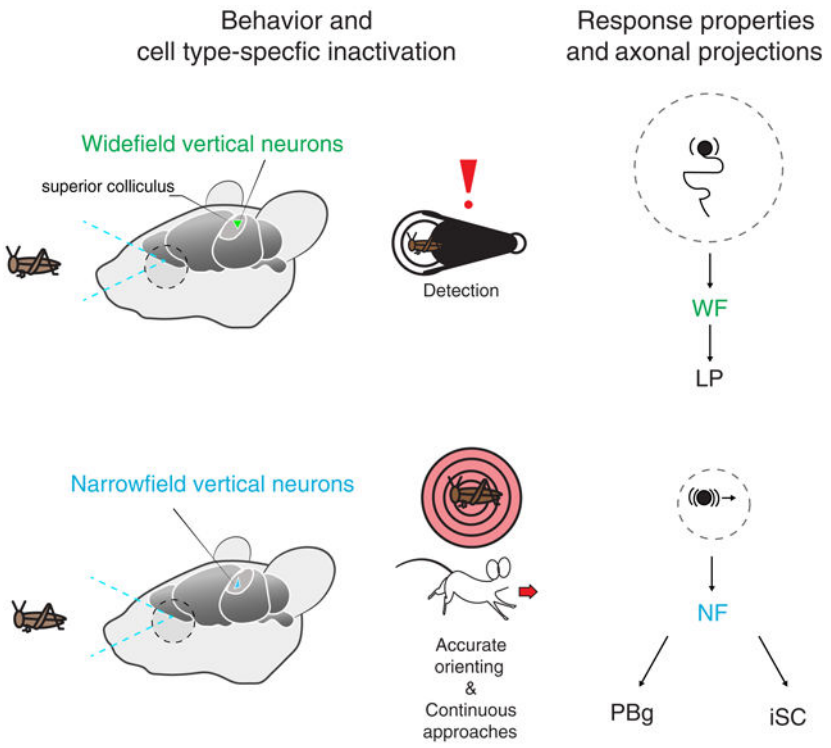

e-TOC

The superior colliculus (SC) plays a conserved role in orienting toward stimuli, but the cell type-specific circuits mediating this are not well understood. Hoy *et al.* study genetically defined cell types of the SC in visually guided prey capture in the mouse, and demonstrate their roles in detecting stimuli versus accurate orienting and approach.

Results

The SC is a laminated structure, with the superficial SC (sSC) receiving multiple sources of visual input, while the intermediate and deeper layers receive multimodal sensory input and project to a broad range of targets and provide motor output [5]. Work in rodents and other species studying the anatomy and visual response properties of sSC cells has advanced our understanding of structure-function relationships of specific neuron types in the mammalian SC [6–9]. In particular, the classically defined wide-field (WF) and narrow-field (NF) vertical cell types [10] have distinct functional and anatomical properties that indicate they may contribute to unique aspects of early visual processing to drive natural approach behaviors. WF cells have large dendritic arbors and respond to small stimuli anywhere within a large region of the visual field, making them ideal for stimulus detection. On the other hand, NF cells have narrow dendritic arbors, are direction selective and respond to stimuli within much more restricted regions of visual space, making them ideal for encoding precise changes in stimulus location. Furthermore, recent genetic studies in the mouse [11] have demonstrated that the WF and NF cells can be independently genetically accessed via

the Ntsr1-GN209-Cre and GRP-KH288-Cre lines, respectively. However, the role of either cell type during natural visual behavior is unknown.

In previous work, we demonstrated that mice use vision to detect, orient towards, and pursue live crickets [12]. The prey capture paradigm therefore provides an opportunity to determine how distinct cell types contribute to visually-guided orienting and approach behavior in a natural context. A recent study demonstrated that neurons in the deeper layers of SC are important for triggering hunting [13]. However, previous work has not directly examined the role of specific cell types in visual superficial SC as they relate to the complex sensory-motor integration that occurs during positive orienting and approach behaviors. Instead, previous studies of the role of specific cell types in superficial SC have only examined innate responses to threatening visual stimuli such as an overhead looming disk [14–16]. These studies showed that a population of parvalbumin-positive (PV) projection neurons was necessary and sufficient to generate behavioral responses related to detection of this stimulus. It remains unclear whether the PV neurons are uniquely engaged by looming stimuli that indicate potential threat, or whether they may be recruited to support positive approach behaviors as well.

Targeted suppression of three populations of cells in superficial superior colliculus

We reasoned that determining how WF, NF, and PV cell types contribute to specific aspects of prey capture would significantly advance our understanding of the circuit mechanisms underlying visual orienting behaviors mediated by the SC. To test the role of these specific cell types in prey capture performance, we used Cre-expressing transgenic mouse lines to target the WF and NF neurons characterized by Gale and Murphy [11] as well as the PV positive neurons that have been shown to mediate responses to threatening stimuli [14,16]. We selectively suppressed the activity of these cells with a chemogenetic approach, employing inhibitory Designer Receptors Exclusively Activated by Designer Drugs (DREADDs) [17]. This approach allowed us to suppress neural activity throughout the course of multiple prey capture bouts, up to several minutes, as opposed to the short timescale control provided by optogenetics. We specifically targeted the inhibitory DREADD, hM4Di (iDREADD), to Cre-positive cells in the superficial SC by virus injection. Viral expression provides spatial localization since Cre expression is found in neuronal populations throughout the SC, as well as other midbrain nuclei and the forebrain, in each of these lines.

Adeno-associated virus (AAV) carrying Cre-dependent hM4Di tagged with mCherry was injected bilaterally into each of the three transgenic mouse lines 2–4 weeks prior to behavioral and physiological testing (Figure 1A & B). At the conclusion of each experiment, we performed histological analysis on brain sections to confirm expression of the iDREADDs throughout the SC, as indicated by mCherry fluorescence (Figure 1A and S1). Expression covered the full rostral-caudal and medial-lateral extent in all three Cre lines (S1A), suggesting a similar distribution for all three cell types. All three lines had a high density of mCherry+ cells in the superficial SC: 94, 80 and 96% of Cre expressing cells in the Ntsr1-GN209, GRP-KH288 and Pvalb-IRES-Cre mice respectively (S1A - D). Few cell bodies were observed in the intermediate and deep layers in each line, and no labeled cells

were found in any other subcortical structures, such PBg or thalamus (S1C & D). A very small number of infected cells were sometimes observed in the overlying cortex in the Pvalb-IRES-Cre mice, probably as a result of the injection needle passing through cortex to deliver virus to the sSC. We confirmed that Ntsr1-GN209 and GRP-KH288 lines do not express Cre in retinal ganglion cells as reported previously [11,18], by performing confocal imaging of flat-mount retinas from crossing each of these lines to a Cre-dependent tdTomato reporter mouse (Ai14). No tdTomato expression was found in retinal ganglion cells, precluding confounds that could be associated with retrograde transport of the iDREADDs to the retina. Taken together, this argues that our manipulations were well-targeted to the superficial layers of the SC.

From the histological sections, we determined the output connectivity of each Cre cell type by measuring their axonal projections throughout the rest of the brain, to aid in the interpretation of the effects of suppression on behavior. Similar to a previous report [11], we found that the WF cell population uniquely sent projections to lateral posterior nucleus (LP, the mouse homolog of pulvinar), whereas the NF population sent projections to intermediate and deep SC, as well as the parabigeminal nucleus (PBg; S1D & E). As previously reported [14,19], the PV population projected to a number of targets, including dorsal lateral geniculate nucleus (dLGN), ventral lateral geniculate nucleus (vLGN), PBg, and patchy projections to intermediate SC (Figure 1A and S1D & E). In addition, we found a previously unreported, dense projection of PV neurons to the anterior pretectal nucleus (S1D & E). Thus, the WF and NF populations have different projection targets from each other, while the PV population has a broad projection pattern that includes strong overlap with the NF targets.

To confirm that systemic injection of CNO was effective in specifically reducing the activity of Cre-dependent iDREADD-expressing neurons, we used optogenetic tagging to identify targeted cells during electrophysiological recording [20]. To tag each of the cell types, we crossed the three Cre lines to the Ai32 line, which expresses ChR2 in a Cre-dependent manner [21]. 2–3 weeks prior to recording, mice from these crosses were injected in the SC with AAV expressing either Cre-dependent iDREADDs-mCherry, or Cre-dependent mCherry only as a control. Using silicon probe recordings in the SC of awake mice, we identified Cre-positive neurons based on their response to 1 ms pulses of blue light. We then measured the mean visually evoked firing rate of neurons, before and after the injection of CNO, during presentation of drifting grating stimuli. CNO injection selectively reduced the mean firing rate of all three cell types within 10 minutes (same interval as behavioral tests) when they were expressing iDREADDs-mCherry, but not when they were expressing mCherry only (median percent change in each group ± the standard error of the median = −1 ± 5%, mCherry only; −35 ± 12%, −39 ± 18% and −42 ± 14%, iDREADD-expressing WF, NF or PV cells respectively, Figure 1C). The mean peak firing rate ± SEM for each cell type prior to CNO injection was, 25 ± 6 sp/s, 9 ± 3 sp/s and 15 ± 6 sp/s, iDREADD-expressing WF, NF or PV cells respectively. We also computed the fano factor (F) as a measure of variability and found no significant changes in F despite firing rate reductions (see Methods). Neighboring Cre-negative cells did not significantly change their firing rate even as Cre-positive cells were suppressed (median percent change in firing rate ± SEM of Cre-negative cells in iDREADDs WF- NF- or PV- Cre mice = −8± 23%, −1 ± 18% and 9 ± 17%,

respectively). These results confirm that CNO is effective in selectively suppressing activity of Cre-expressing neurons in each transgenic line, without significantly impacting the stimulus driven responses of other cell types in sSC. We note that in addition to reducing excitability directly, iDREADDs also strongly reduce synaptic neurotransmitter release [22], which results in even greater efficacy in suppressing each cell type's contribution to behavior than observed in firing rate alone.

Suppression of WF and NF cells differentially affects specific aspects of prey capture

In order to test the role of each of the three cell types in orienting behavior, we measured prey capture performance following iDREADD-mediated suppression via injection of CNO. All mice were habituated to the arena, handlers, and crickets after they recovered from the virus injection and before their first injections with CNO (Figure 1B). We compared the performance of each Cre line expressing iDREADDs in a given cell type to a single control group comprised of combined data from all three Cre lines expressing mCherry alone. All groups, including controls, received an injection of 1 mg/kg CNO 10 min prior to behavioral assessment. Thus, any potential non-specific effects of CNO would be shared across experimental and control groups.

Following CNO injection, we found significant changes in prey capture behavior that led to overall increases in the average time to capture prey for mice with WF or NF cells suppressed by iDREADDs relative to controls (Figure 2A–E), but no effect of suppressing PV cells relative to controls. Time to capture was defined as the time between introducing the cricket and when the mouse captured and began to consume the cricket. Although suppression of WF and NF neurons increased the time to prey capture, all mice tested eventually captured and consumed each cricket they were given within 7 minutes on each trial (Figure 2, Videos S1–4). We confirmed that median capture times for control mice injected with CNO (6.05 ± 2.70 s) were no different from mice injected with saline the day prior (9 ± 2 s, 7 ± 2 s, 5 ± 1 s, 6 ± 2 s, control, WF, NF and PV groups, respectively), demonstrating that neither the injection procedure nor CNO itself impairs prey capture performance.

To determine the distinct impairments in prey pursuit for each group of mice, we visualized individual approaches that we defined based on mouse speed and distance from target (range) relative to the cricket (Figure 2A–D), as previously described [12] (and see Methods). Briefly, approach starts were defined as moments where the azimuthal angle of head relative to cricket location was within 90 deg, the range began to continuously decrease, and the mouse was moving at greater than 3 cm/s. The approach continued for as long as all behavioral criteria described above were met, or until the mouse made contact with the cricket (range < 3 cm). Under normal conditions, it takes less than 5 s from cricket introduction to when mice begin their first approach and complete a successful contact event (Figure 2A–A"', Video S1). If an initial contact does not result in capture and consumption, they resume pursuit in less than 1 second and mount another approach.

When the activity of WF cells was suppressed (Video S2), mice took longer to detect the cricket, initiate their first approach (Figure 2B"), and started approaches closer to the target (Figure 2B"', versus Figure 2A"), but were successful in pursuit following initiation (Figure

2B”’). Strikingly, when the activity of NF cells was suppressed (Video S3), mice showed deficits in orienting toward the cricket, were less accurate during their approach, and often stopped their pursuit, becoming immobile before intercepting the cricket (Figure 2C’–C”’). When PV cells were inhibited (Video S4), mice made the rapid, precise and distant approaches observed in control conditions (Figure 2D–D”’ versus Figure 2A–A”’). Together these changes in approach and pursuit lead to significant differences in time to capture between groups (Figure 2E).

To precisely quantify the deficits caused by suppression of WF or NF cell activity, we assessed distinct aspects of the prey capture behaviors that rely largely on vision [12]. In particular, we calculated parameters to assess a) detection, b) accuracy of approach, and c) continuity of pursuit.

We first quantified two measures associated with *prey detection*: time to first approach (as defined above), and range when an approach started. Suppressing the activity of either the WF or NF cells increased the average time to first approach prey relative to both controls and mice with suppressed PV neuron activity (Figure 3A, top). These results indicate that suppressing WF or NF cells impairs prey detection, as measured by the ability to initiate approaches. We note, however, that this could be due to either failure to detect the stimulus, or failure to execute the orienting that is our measure of detection. Interestingly, control mice tended to start a successful approach from either approximately 10 or 30 cm away from the target, as the approach start distribution was bimodal (see Methods, Figure S3A). In control mice, most first approaches were started farther than 15 cm away from the target (Figure 3A, bottom). Notably, mice with suppressed WF cells specifically showed a significant decrease in the probability of starting approaches from greater than 15 cm away from target (Figure 3A, bottom and Figure S3B), whereas inhibiting NF (Figure S3C) or PV cells yielded no change in average start location. In addition, we examined bearing relative to the target 500 ms prior to approach start and found that the distribution for this metric is also bimodal in control mice (Figure S3D). Mice tended to start approaches at bearings of either 12 ± 10 or 75 ± 16 degrees, i.e. with the cricket directly in front of the mouse, or lateral to the mouse. The WF mice displayed significantly different orienting behavior and were more likely to respond to targets directly in front, less than 40 degrees (Figure S3E). Taken together, this suggests a specific role for WF cells in stimulus detection, particularly at farther distances and in the periphery.

Second, we quantified the *accuracy of targeting* by comparing bearing during an approach, and the probability of successfully intercepting the cricket given an approach. Only suppressing the activity of NF cells decreased the accuracy of targeting in both of these measures once approaching began (Figure 3B). This suggests that mice with NF cell activity suppressed in the sSC fail to orient accurately. This could be due to inability to orient, or, lack of orienting due to other behavioral factors. Regardless, these findings suggest that NF cells in sSC play a unique and critical role in accurately targeting prey, relative to the other cell types investigated here.

Third, we quantified the ability of mice to consistently maintain pursuit of the prey (*pursuit continuity*). We observed that suppressing the activity of NF cells often resulted in mice

pausing shortly before prey contact during an approach, when they were within 5 cm of the target (Figure 3C, top and Figure 2C"', clustered track points near target position). These mice were also less likely to continue pursuit by re-initiating an approach within 1 second after the cricket escaped a contact event (Figure 3C, bottom). These differences in pursuit continuity were unique to suppressing the activity of NF cells and indicate that this population of cells is critical in driving and maintaining accurate motor behaviors during pursuit and ensuring rapid prey capture.

Quantification of the density and distribution of labeled cells in each experimental group suggests that the effects of neuronal inhibition on behavior are cell type-specific. In all lines, the majority of neurons in each Cre+ cell type were labeled by viral expression (S1C). Correspondingly, a similar total number of cells expressed hM4Di in the PV and WF groups, while the NF group had half as many cells expressing hM4Di since this Cre line is not as dense (S1A–D), yet had more significant and distinct behavioral impairments relative to the other two groups. Furthermore, our electrophysiological recordings showed a similar degree of suppression of firing rate per cell (~35–42%) following CNO administration in these three groups (Figure 1C). Therefore, the extent of the behavioral phenotype does not correlate directly with the number of cells expressing iDREADDs nor to differences in the percent reduction in stimulus evoked firing rate after CNO administration. The PV cells also overlap in the location of their cell bodies with both the WF and NF cells (Figure 1A and S1A), and some of their projection targets overlap with that of the NF cell population (Figure 1A and S1D & E). Despite sharing these anatomical properties with NF neurons, suppressing the activity of PV cells had no impact on our measures of prey capture behavior (Figure 2 & 3). As there were nearly 3x as many total PV cells inhibited by iDREADDs as NF cells, this also suggests that the effects on behavior are cell type-specific and unlikely to be caused by regional suppression of activity in SC or other projection target areas.

To determine whether the observed phenotypes were a result of general disruption of motor behavior or other state changes such as anxiety, we analyzed running speeds and exploratory behavior in the open field in the absence of live prey after CNO injection. We did not identify any differences between experimental groups and controls in maximum and mean speeds of locomotion, time spent within the perimeter of the arena, or percent time immobile (S2). None of our manipulations significantly affected the probability of capturing the cricket given an attack, suggesting that attack behaviors relying on touch or whisking were unaffected by our manipulations (probability of capture given contact was 38 ± 16%, 32 ± 4%, 20 ± 5%, and 33 ± 7%, control, WF, NF or PV mice, respectively). Taken together, these findings suggested that specific aspects of visuomotor behaviors are differentially affected by the selective suppression of these three cell types in sSC. The WF and NF neurons manipulated here are specifically required for some unique behaviors relevant to prey capture, while PV cells in sSC play little or no role under the conditions tested here.

Visual responses of identified cell types are consistent with their role in prey capture.

We next sought to determine how the visual function of each cell type relates to its role, or lack thereof, in prey capture. In a previous study, the visual stimulus response properties of both the WF and NF cells in these Cre lines were characterized in anesthetized mouse [11],

whereas there has been characterization of the WF and PV response properties with more limited stimuli in the awake mouse [14,16,23]. In order to provide a systematic comparison across all three cell types we quantified a range of visual response properties in awake mice by performing acute extracellular single-unit recordings with silicon multisite electrodes while applying the optogenetic approach described above to identify Cre-positive neurons during recording (Figure 4A). We presented sparse light and dark spots of a range of diameters, either stationary or moving at a range of speeds [24]. These stimuli enabled the quantification of spatial receptive fields via reverse correlation, ON/OFF response polarity, size and speed selectivity, and responsiveness to moving stimuli. In addition, we presented drifting sinusoidal gratings to measure orientation and direction selectivity as previously described [25].

Quantifying the visual response properties of the WF, NF and PV neurons to the same stimulus set confirmed that the targeted WF and NF populations have distinct response preferences from each other and from PV cells (Figure 4C–H). Figure 4C shows representative responses from the three cell types and demonstrates that all cells show robust responses to relatively small, moving stimuli. WF neurons have the largest receptive field sizes (Figure 4E), consistent with finding that they respond to small sparse stimuli anywhere within a relatively large area of visual space. They respond to both light (ON) and dark (OFF) spots and have the strongest preference for moving stimuli, as they are the least responsive to flashing stimuli (Figure 4D). They are also the most speed selective, with a significantly greater fraction of cells exhibiting speed selective responses to moving stimuli (87.5 ± 8%, 57.1 ± 12% and 56.3 ± 12%, WF, NF and PV cells, respectively. n=16, 14 and 16, χ^2). On the other hand, the NF neurons have much smaller receptive field sizes than the other two cell types (Figure 4C & E) and are direction selective (Figure 4F). While the same types of information were conveyed by subsets of the PV population, this population was not direction selective, had a substantial fraction of neurons with only OFF responses and a preference for larger sizes than NF and WF cells. Importantly, all populations exhibited relatively high levels of size selectivity (87.5 ± 8%, 85.7 ± 9% and 68.8 ± 12% of WF, NF and PV cells, respectively).

Overall, the receptive field properties of the WF and NF neurons, as measured here and in previous studies, mapped well to their roles in prey capture behavior. WF cells encoded small (4–5 deg) light or dark objects moving within a large region of the visual field, consistent with detecting the presence of a stimulus. In contrast, the NF cells responded to small light or dark spots within a much smaller region of visual space, and were tuned to the direction of stimulus movement, information that is important for guiding approach toward a target. The PV cells responded to larger and often dark stimuli, and while we did not find a role for the PV cells in prey capture behavior here, these response features are consistent with their previously demonstrated role in mediating fear response to looming stimuli.

Discussion

Our findings connect genetically identified cell types in sSC and their visual responses in the alert mouse to specific aspects of prey capture behavior. We found that suppressing WF neurons disrupted rapid prey detection but left other aspects of prey capture unperturbed,

such as accurate orienting and continuous approaches. This disruption in detection is consistent with the observation that WF neurons have large receptive fields, are selective for stimulus size, are most responsive to moving stimuli, and project exclusively to lateral posterior nucleus. The selectivity for small objects anywhere within a large receptive field could provide sensitivity for stimulus detection, with less specific information about stimulus location or direction of motion. However, it should be noted that although individual WF neurons do not encode location with high precision, a population of many neurons with significantly overlapping RFs could provide an accurate estimate of the spatial location of a small moving object [26].

Furthermore, the WF neurons project to LP, the mouse homolog of pulvinar, which could convey the detection signal to cortex as an “alert” for salient stimuli. Previous studies of LP have demonstrated that neurons in this higher-order thalamic nucleus encode visual stimuli over a large region of the visual field, as well as contextual information [27]. Information carried by WF cells to LP is then relayed to specific areas of extrastriate visual cortex by circuitry that operates in parallel to the classical retino-geniculate pathway to cortex [23,28]. While it remains unclear how information along this pathway is integrated with visual processing occurring along the retinogeniculate pathway, we speculate that it could serve to shift cortical processing towards newly detected stimuli. Together, our findings support the idea that WF cells in sSC provide rapid initial detection of stimulus presence and can convey this information to extrastriate cortex via higher-order thalamus.

On the other hand, we demonstrated that suppressing NF neurons impaired accurate targeting and continuous pursuit behaviors. These neurons respond best to stimuli localized within small regions of the visual field, are direction selective, and project directly to intermediate/deep SC and the parabigeminal nucleus (PBg). The small receptive fields and direction selectivity of NF neurons are consistent with the information needed to drive an accurate motor output to the location of a moving target. Moreover, the deep SC neurons they project to are topographically organized such that they can direct eye or head movements towards a particular region in visual space by driving downstream brain regions involved in motor output [29–31], and likewise these deeper SC neurons have recently been shown to drive prey capture via a projection to zona incerta (ZI) [13]. Furthermore, interactions between SC and PBg (or its non-mammalian homolog, the isthmic nuclei) have been shown to create a competitive amplification circuit based on inhibitory and cholinergic mechanisms that is involved in selecting one target within the visual field [4,32,33]. Providing input to both deep SC and PBg could therefore simultaneously guide motor output during approach and facilitate selection/pursuit of a single target. Thus, our findings are consistent with NF cells driving the visually-guided motor output needed for continuous and accurate targeting of prey.

Finally, suppressing the population of cells in sSC targeted in the PV-Cre line had no significant effect on prey capture. These neurons consistently responded to larger, often dark, moving stimuli, and projected to a number of targets including pretectal nuclei as well as the intermediate/deep SC and PBg. They also project to the dLGN, and recent studies have shown that this tectogeniculate pathway primarily targets the shell of the dLGN, which in turn directly targets superficial layers of V1, providing another distinct route for stimulus

information to be transmitted to cortex [34,35]. Though the population of PV+ cells is diverse morphologically, and a subset of their projection targets overlap with that of the NF population [19], our data taken together with previous studies of this cell type are consistent with the idea that these cells contribute to threat detection and associated behavioral responses [14], as opposed to prey capture. Thus, distinct circuitry in sSC is required for visual processing that drives different behavioral outputs associated with specific ethologically relevant visual stimuli.

Notably, we did not observe direct projections from any of the superficial SC cell types studied here to the zona incerta (ZI), central amygdala, or periaqueductal grey, all regions recently shown to play a role in driving prey approach or prey attack [13,36–39]. This suggests that the sSC cells must first convey the relevant visual information to intermediate targets, such as the intermediate or deep SC, in order to ultimately drive prey capture behavior.

The impact of our cell type-specific manipulations was likely restricted to visual processing, rather than other sensory modalities, as the iDREADD expression was primarily targeted to superficial SC, which receives visual input and does not have multisensory responses [40]. In addition, the aspects of prey capture that were disrupted here, such as approach initiation and accuracy of orienting, were the same aspects previously found to be dependent on vision [12]. On the other hand, aspects of prey capture that were not found to be vision-dependent, such as short-range pursuit and probability of capture after contact, were not disrupted by suppression of superficial WF and NF cells. It remains possible that more detailed measures of specific features of these behaviors might reveal further deficits, such as in the accuracy of biting during capture [37].

This study does not address the possible role of cortex in prey capture, as our goal was to use prey capture to probe the neural circuits for visually-guided orienting and approach in the SC. However, V1 and other cortical areas provide significant input to SC that can modulate both neural activity in SC and behavioral output [41–43]. In addition, one recent study has shown an impact of V1 suppression on rapid prey capture [36]. It will be interesting in future studies to further probe the role of specific cortical circuits in mediating distinct aspects of prey detection and approach behaviors mediated by vision such as those analyzed here.

In summary, these findings significantly expand our understanding of how visual processing in the SC relates to robust, conserved ethological behavior. This opens up new directions of research studying the mouse superior colliculus to understand further aspects of approach behavior such as rapid object identification, stimulus valence assignment, target selection, behavioral choice and sustained pursuit of targets. Importantly, it is also well established that SC, particularly in higher mammals is required for more complex visuomotor and even cognitive functions, such as spatial selective attention (for recent reviews see [3,9]). This study begins to clarify our understanding of SC visual processing in this context by identifying specific cell types that are differentially required for aspects of visually-guided locomotor orienting. Similar processes are likely to be engaged in attentional orienting as well [4], and recent work has demonstrated that mice perform visual selective attention tasks

reliably [44]. Thus, it will be interesting to determine to what extent the cell types and circuits described here play specialized roles in mediating rapid innate behaviors, or more general roles in attentional gating and salient stimulus selection across behavioral contexts.

STAR ★ Methods

Lead Contact and Materials Availability

Further information and requests for resources should be directed to and will be fulfilled by the Lead Contacts, Cristopher Niell (cniell@uoregon.edu) and Jennifer Hoy (jhoy@unr.edu). This study did not generate unique reagents.

Experimental Model and Subject Details

All studies were conducted with approved protocols from the University of Oregon Institutional Animal Care and Use Committees, in compliance with National Institutes of Health guidelines for the care and use of experimental animals.

Adult male and female transgenic mice were used in this study (2–5 months of age). We used the following Cre transgenic lines to isolate and manipulate specific cell types in the superior colliculus: Grp-KH288-Cre and Ntsr1-GN209-Cre [18], and Pvalb-IRES-Cre [45]. In a subset of experiments each of these Cre lines were crossed to Ai32 mice in order to express channelrhodopsin-2 (ChR2) in Cre-labeled cells [21] The mice were housed under a 12 h light/dark cycle and non-food deprived mice were provided with food and water *ad libitum*. Food trays were removed 12–24 hours before prey capture testing.

Method Details

Virus delivery—To target the expression of inhibitory DREADDs or fluorescent tags to specific populations of cells in the superior colliculus (SC), we injected AAV8-hSyn-DIO-hM4D(Gi)-mCherry [46] or AAV8-hSyn-DIO-mCherry (gift from Bryan Roth, addgene plasmid #50459) virus bilaterally into the superficial SC of Cre-transgenic mice 2–4 weeks prior to behavioral or physiological recording experiments. 0.25 μl of virus was injected at a rate of 0.1 μl/min into each of two burr holes in each hemisphere of the skull along the following coordinates (from lambda/lateral from midline, and depth; in mm): A0.2/L0.9 and A0.0/L1.1, and D: 1.2 [47]. All mice received preoperative analgesia: 5 mg/kg Carprofen (subcutaneous), lactated ringers for hydration (subcutaneous) and anesthetic: 1.5–2% Isoflurane throughout the procedure. Injections were performed with a Nanoject II (Parker, Inc.) fitted with pulled glass pipettes. Surgical sites were fully healed and sutures removed by 1–2 weeks post injection.

Histology—Fluorescent signals were obtained from 80μm coronal sections of 4% PFA fixed brains. Brains were imaged using a Zeiss Axio Imager 2 microscope. Images taken with the 2.5X objective were used to quantify fluorescent signals of specific brain regions. We quantified fluorescence expression (cells and projection densities) from sectioned tissue spanning 0.5 to −5.0 bregma. To capture the mCherry fluorescent signal, we used the 1114–101 FL Filter Set 43 from Zeiss. For images, exposure times were generally set between 1000–1500 ms, with 1x analog gain.

Fluorescence images were analyzed using ImageJ analysis software. Each image was converted to 16-bit grayscale and ROIs were drawn around each of the analyzed structures: LP, dLGN, vLGN, APT, PBg and the SC. Structures were identified based on Paxinos and Franklin [47], and subregions and laminae of SC were defined as in Comoli et al [48]. We then applied the ImageJ background subtraction function (rolling ball radius set to 12 pixels) and thresholded the image to select the total area containing fluorescent signal. We took the area fraction measure, which is the percentage of pixels in the selected ROI above threshold with significant fluorescent signal. An additional control ROI was drawn around a portion of each section outside of potential target areas in order to quantify signals due to autofluorescence. We quantified three representative sections approximately 80–240 μm apart through each area in each subject depending on the size of the structure. Cell counts were performed in a semi-automated fashion as in Tervo et al [49]. Given that labeled cells populated laminar structures, we quantified cell counts as the number of objects isolated along a 1mm long line drawn through the center of mass of the labeled cell population (S1B, bottom panel). We imaged and quantified mCherry positive cells and/or projection fluorescence from 0.5 anterior of bregma to - 5.0 posterior of bregma.

Behavioral testing—Approximately one week prior to assessment of prey capture performance, mice were habituated to handlers, prey capture arena, and prey (house crickets, Fluker's Farm) as described previously [12]. Experimental assessment began once mice consistently performed prey capture behavior within the arena following food deprivation, with an average capture time of less than 30 s. In order to habituate to i.p. injection, mice from all treatment groups were given an i.p. injection of saline 5 min prior to a 5 min habituation period in the arena followed by 4 prey capture trials. On the second day of saline injection, behavior was recorded and capture times for the first three prey capture trials post-injection were averaged to confirm that capture times were similar to baseline performance for each animal. The day after saline injection habituation, the same mice were all given i.p. injections of clozapine-N-oxide (CNO) at 1 mg/kg prior to arena habituation and 4 subsequent prey capture trials. All behavioral data reported here are from the first 2–3 prey capture trials, recorded within 10–40 min after CNO injection. To control for possible non-specific effects of CNO, we compared all groups to CNO injected mice from all three Cre lines expressing only Cre-dependent mCherry. Thus, our controls were virus injected and were given CNO, but expressed only the fluorophore.

We quantified prey capture behavioral performance as described previously [12]. Briefly, mice performed prey capture in a rectangular, white acrylic arena 45 cm long × 38 cm wide × 30 cm high with vinyl flooring. The arena was evenly illuminated from above, with luminance measured to be 60 cd/mm^2. Video recordings were initiated prior to the introduction of the cricket. The experimenter held crickets in both hands and crickets were placed in different parts of the arena. While distracting the mouse with one hand, the insect was quietly released by the opposite hand that was not approached by the mouse. This minimized the possibility of mice employing initial localization strategies based on sound or visual cues unrelated to the prey, such as the hand of the handler. Capture time was taken as the time from the removal of the experimenter's hands until the mouse had captured and

begun to eat the cricket. The floor of the cage was cleaned between each trial and mice participated in four sequential capture trials on testing days.

Behavior was recorded at 60 frames per second with a high-resolution area scan camera (2048 × 1088 pixel; model ac2000–165umNIR, Basler). We digitized the 2-dimensional position of the cricket, the center of mass of the mouse's body and each of the mouse's ears (colored green with non-toxic marker or body paint) using a custom written MATLAB based algorithm courtesy of Dr. Tristan Ursell. From this tracked data, we then extracted the mouse's head direction relative to the cricket, target speed, mouse speed and range (distance in cm between prey and mouse). The center of the mouse's head position was defined as the midpoint between the two ears, and head direction/bearing was defined as the vector perpendicular to the line between the two ears. From these measures we determined head position and locomotor speeds as a function of prey position over the course of each prey capture trial. All range and bearing data were smoothed via a 50 ms sliding average window to filter out measurement noise that did not reflect the overall trajectory of the animals.

Similar to our previous studies, we defined the start of approaches as times during the capture trial when the mouse was moving at speeds greater than 3 cm/s, the range relative to the prey was steadily decreasing (Δ Range < −1cm over 50 ms), and the mouse maintained an azimuth of < 90°. We defined the termination of the approac h as the moment when the mouse came into contact with the prey (defined as range < 3 cm), or when any of the initial approach criterion deviated for more than 250 ms. To control for nested data effects, we first averaged each individual's performance over a similar number of trials and then compared the mean or median of each group (except where indicated). For binominal (probability) measures, the mean (μ_p) was equal to the probability of success (P) / number of trials (n). The standard error of the sampling distribution was computed as the standard deviation (σ = sqrt(PQ)) divided by the normalized sample size (sqrt(n)), where Q is the probability of failure, 1-P. Probability measures identified as successes in this study were: 1) if a mouse captured a cricket within a 5 min prey capture trial, p(Capture Success), 2) if a given approach towards prey ended in prey contact (end approach distance < 3 cm of prey), p(Interception |Approach), and 3) if an interception lead to the final capture, p(Capture| Interception).

In vivo electrophysiology—Multisite silicon probe recordings in awake head-fixed mice were performed as described previously [50]. Briefly, mice were first implanted with a stainless steel headplate 2 days prior to recording. The headplate allowed head fixation atop a spherical treadmill (adapted from [51,52], which permits free locomotion during visual stimulus presentation and electrophysiological recording. To implant headplates, mice were anesthetized with isoflurane in oxygen (3% induction, 1.0–2% maintenance), warmed with a heating pad at 37°C and given subcutaneous injections of 0.25 ml lactated Ringer's solution and Carprofen (5 mg/kg). In all animals, the scalp and fascia from Bregma to 2 mm behind Lambda were removed, and the skull was covered with a thin layer of cyanoacrylate (VetBond; WPI) before attaching the head plate with dental acrylic (Ortho-JET; Lang Dental Manufacturing). The well of the head plate was filled with silicone elastomer (Kwik-Sil; WPI) to protect the skull before recordings.

On the day before recording, the animals were anesthetized to perform a craniotomy over the anterior superior colliculus. The craniotomies were ~2 mm in diameter and centered at 2 mm lateral of midline and 0.5 mm anterior of the posterior suture. The brain surface was covered in 1.5% agarose (Sigma-Aldrich) in sterile saline and then capped with silicone elastomer during an overnight recovery. After removing the protective agarose and silicone plug, the ground wire was set, and a fresh layer of 1.5% agarose in saline was applied to the well. We next inserted a 32 site, linear array optotrode (A1×32-5mm-25-177-OA32LP; Neuronexus Technologies), with 25μM site spacing and a 50μM, 0.22 NA optic fiber located ~200μM superficial to the top electrode site. The tip of the electrode was coated with DiD (Invitrogen) to allow *post hoc* track recovery. To access the superficial SC, the optotrode penetrated overlaying V1 and was advanced until units responsive to flashing spot stimuli were observed. After the appropriate depth was reached, agarose was added to stabilize the electrode, and the preparation was allowed to settle for 40 min while the animal was shown stimuli and thresholds were set. Only one penetration per animal was used in the final analysis. All units stably isolated over the recording were included in subsequent analysis, with specific response properties calculated offline. Recording sessions typically lasted ~2 hours and proceeded as follows: one minute light-mediated identification of Cre-dependent ChR2 expression to identify sites with ChR2 positive neurons, 20 min recording of unit responses to drifting grating stimuli, 20 min flashing spot movie stimulus, 20 min moving spot stimuli, 4 min light-mediated identification of ChR2 positive units session, a CNO or saline injection followed by 10 min settling period, and lastly, a 45 min drifting grating stimulus session to quantify post injection cellular activity. To determine the efficacy of CNO mediated shutdown in targeted cell types, the mean firing rate was calculated across all presentations of stimuli during the drifting grating presentation, pre- and post-CNO or saline administration.

After the recording session, mice were deeply anesthetized in 3% isoflurane and euthanized via cervical dislocation. The brains were then fixed whole in 4% PFA (Electron Microscopy Sciences) overnight at 4 °C. Brains were subsequent ly sectioned and mounted in Fluoromount G with DAPI (Southern Biotechnology). We imaged the DiD electrode tracks on a Zeiss Axio Imager 2 to confirm that penetrations were specific to the target SC lamina.

Optogenetic identification of Cre positive neurons—To identify the Cre-positive cells during electrophysiological recordings, we crossed each of our Cre lines to the Ai32 line, which expresses ChR2 in a Cre-dependent manner. This allowed optogenetic tagging of our targeted cell populations [20,53,54]. We delivered light near the recorded neurons via an optic fiber attached to the optotrode, from a 473nm (blue light) diode-pumped solid-state laser (OEM Laser Systems, 200 mW). The presence of ChR2 positive neurons near the optotrode was first confirmed prior to recording with a brief 1 min total duration stimulation protocol whereby 1 ms long pulses of blue light were delivered at a frequency of 5 Hz for an on-period of 3 sec followed by an off-period of 3 sec. Inspecting the multiunit activity aligned to light pulse onset revealed that light-evoked neuronal activity was restricted to sites and depths consistent with the known expression of Cre-recombinase in our different lines. After recording responses to all visual stimuli, we ran the light-stimulation protocol as described above for 3 separate sessions where we varied the laser driver current (power of

light illumination at the tip of the optic fiber). Light intensity at the location of the recorded neurons was estimated by measuring light power at the tip after the recording and using the calculator provided by the Deisseroth lab (https://web.stanford.edu/group/dlab/cgi-bin/graph/chart.php). Based on power emitted at the tip of the fiber at the settings used in our experiments, light intensity at recorded sites ranged from between 30–70 mW/mm^2 with an average intensity of 41 ± 6 mW/mm^2 at approximately 200 μm from the tip. The overall duration of a session at each power was 4 min to allow for an ample number of trials to derive robust measures of reliable light-evoked neuronal responses (See Figure 4A). Units that reliably followed with a latency of less than 1.5 ms and a jitter of less than 1.5 ms across all trials after the onset of each laser light pulse were identified as putative ChR2 positive neurons and inferred to be from the targeted Cre-positive neuron population in each subject.

Visual Stimuli—Visual stimuli were presented as described previously [25]. Briefly, stimuli were generated in MATLAB (MathWorks) using the Psychophysics Toolbox extension [55,56] and displayed with gamma correction on an LCD monitor (Planar, 30 × 50 cm, 60 Hz refresh rate). The screen was placed 25 cm from the mouse's eye, subtending ~60–75° visual space. Monitor mean luminance was measured to be 50 cd/m^2. The monitor was centered on the hand-mapped RF location of multiunit activity.

To characterize selectivity of single-unit neural responses, we presented drifting sinusoidal gratings of 1.5 s duration at 100% contrast, with temporal frequency of 2 Hz, SF of 0.01, 0.02, 0.04, 0.08, 0.16, 0.32, and 0 cycles/° (cpd) in 12 evenly spaced directions. Gratings with a temporal frequency of 2 Hz were chosen to compare responses with those from a previous study (Gale and Murphy 2014), which showed that a temporal frequency between 1–3 Hz captures most selective responses of specific cell types in sSC. The spatial frequencies were randomly interleaved, and a gray blank condition (mean luminance) was included to estimate the spontaneous firing rate. In most cases, the spatial RF size was estimated by the spike-triggered average (STA) in response to sparse flashing noise, as described previously [24]. The sparse flashing noise movie consisted of ON (full luminance) and OFF (minimum luminance) circular spots on a gray background, at a density such that on average 15% of the area on the screen was covered on any given frame. Spots were 2, 4, 8, 16, and 32° in diameter, and presented such that each size made up an equal fraction of the area on the screen (e.g., number of spots was inversely proportional to their area), to ensure even coverage at each point in space by every size. In addition, 20 frames each of full-screen ON and OFF were randomly interleaved. Each movie frame was presented for 250 ms followed by immediate transition to the next frame, for a total duration of 20 min. Size tuning curves were generated based on the firing rate during each stimulus presentation when a spot overlapped the receptive field [24]. Units were defined as size selective if they had a peak response greater than 1.5 sp/sec relative to neighboring sizes in the tuning curve. Preferred size was then defined as the peak of selective tuning curves (Figure 4C).

We mapped stimulus speed selectivity using a sparse moving noise stimulus [24]. Briefly, this stimulus also uses ON and OFF spots, with a more limited size range (4, 8, 16° diameter), but each spot was assigned to move in one of eight evenly spaced directions and one of 5 speeds (10, 20, 40, 80, 160°/s). Spots appeared on the app ropriate edge of the screen and moved across until they disappeared on the far edge. The movie was presented

for 20 min total duration. Size and speed tuning curves generated from these stimuli were also robust, with selective and peak response defined as above. In the case where a cell responded to both flashing and moving stimuli well, both stimulus sets yielded peak responses to similar sizes.

In some cases, subsets of WF and NF cells responded poorly to flashing stimuli (Figure 4D), but did respond well to sparse moving stimuli, as in previous studies [11]. Therefore, in a subset of experiments we used a sparse, moving stimulus to estimate the RF size and confirm stimulus size selectivity for all cell types.

Electrophysiological Data Acquisition—Signals were acquired using a System 3 workstation (Tucker Davis Technologies) and analyzed with custom routines written in MATLAB [24,50,51]. For single-unit activity, the extracellular signal was filtered from 0.7 to 7 kHz and sampled at 25 kHz. Single-unit clustering and spike waveform analysis was performed as described previously [25] with a combination of custom software in MATLAB and Klusta-Kwik [57]. Typical recordings yielded ~6–10 single units. Most units appeared predominantly on a single recording site, although units often contributed a signal below the voltage threshold on neighboring sites, which allowed improved unit discrimination. Unit jitter was taken as the variance of the spike count divided by the mean spike count 1.5 second after multiple presentations of the preferred stimulus, the fano factor (F), or, $F=\sigma_w^2/\mu_w$ where w = 1.5 sec post stimulus.

Quantification and Statistical Analysis

All statistical tests, significance levels and samples sizes are reported in the figure legends. For all datasets, we inspected for the presence of outliers, multiple modes, or skews in order to determine whether to use parametric or nonparametric approaches for tests of statistical significance. In most cases we include the full distribution of each dataset. For distributions that appeared bimodal, such as approach start distances and the average head angle prior to approach, we fit distributions using MATLAB's Statistics and Machine Learning Toolbox function as a mixture of two gaussians. This fitting yielded parameter estimates, means and standard deviations, for each mode. This allowed us to compute Ashman's D, and D>2 was taken as evidence of bimodality and clear separation of modes. To determine the threshold for categorizing an event as belonging to the first mode or the second, we determined whether a value was less than the mean of the first mode plus at least 2 standard deviations (part of the first mode). In the case of the approach starts distribution, the mean estimate of the first peak was 9.6 with a SD of 1.5 cm, while the mean estimate of the second peak was 31.8 with an SD of 9.4 cm. We set our threshold for distant approaches as starting from greater than 15 cm from target as this was where we observed a clear dip in the distribution histograms and it was greater than 2 SDs above the mean of the first mode. Similarly, we thresholded "direct" bearings as those occurring less than 40 degrees. The first mode was 12 degrees with a standard deviation of 10 degrees. Thus, 40 degrees was where we both observed a clear dip in the distribution histogram and is greater than 2 SD from the mean of the first mode. We also performed Kolmogorov-Smirnov tests to detect significant differences in the distributions.

To compare means of unimodal, normal distributions, we used one-way (genotype) ANOVA followed by Tukey-Kramer HSD post hoc testing. To detect significant differences between medians, we used Kruskal-Wallis omnibus testing, followed by pairwise Mann-Whitney U tests. In some cases, we employed the Wilcoxon signed rank test to determine whether measurements significantly deviated from 0 in each tested group. Alpha in all cases was set to 0.05 and significance was inferred if p values were less than 0.05, indicated by asterisks in figure legends. Standard Error of the Median (SEM) was obtained via a bootstrapping procedure (data sampled 1000x). For all experiments we report number of trials or cells (n) as well as the total number of independent animals in each experiment in the figure legends. Unless otherwise noted, we control for nested effects by computing statistical analysis on average measures from each animal. In all cases, we also minimized nested effects by obtaining similar number of cells or trials from each animal. We typically obtained 2–4 cells or behavioral trials from each animal. Differences in frequency of categorical observations between groups were determined via χ^2 test.

Data and Code Availability

Raw behavioral video data, Matlab data files with processed mouse/cricket tracks, and related Matlab code are all available at http://www.hoylab.com/publications.html.

Supplementary Material

Refer to Web version on PubMed Central for supplementary material.

Acknowledgments

We are indebted to Drs. Martha Bickford, Samuel G. Solomon, Clifford Keller and Judith Eisen, and members of the Niell and Hoy labs, for helpful discussions and comments on drafts of the manuscript. We also thank Mandi Severson for extensive work obtaining and imaging histological data, and Dr. Tristan Ursell for Matlab code that facilitated color-based tracking of mouse and cricket. Dr. Travis Wiles kindly provided the original graphic of mouse viewing cricket which we modified for our graphical abstract. This work was supported by NIH grants F32EY24179 (JLH), P20GM103650 (JLH), and R01EY023337 (CMN).

References

1. Dean P, Redgrave P, and Westby GWM (1989). Event or emergency? Two response systems in the mammalian superior colliculus. Trends Neurosci. 12, 137–147. [PubMed: 2470171]
2. Wurtz RH, and Albano JE (1980). Visual-motor function of the primate superior colliculus. Annu. Rev. Neurosci 3, 189–226. [PubMed: 6774653]
3. Krauzlis RJ, Lovejoy LP, and Zénon A (2013). Superior colliculus and visual spatial attention. Annu. Rev. Neurosci 36, 165–182. [PubMed: 23682659]
4. Knudsen EI (2018). Neural Circuits That Mediate Selective Attention: A Comparative Perspective. Trends Neurosci. 41, 789–805. [PubMed: 30075867]
5. May PJ (2006). The mammalian superior colliculus: laminar structure and connections. In Progress in Brain Research, pp. 321–378.
6. Ito S, and Feldheim DA (2018). The Mouse Superior Colliculus: An Emerging Model for Studying Circuit Formation and Function. Front. Neural Circuits 12, 10. [PubMed: 29487505]
7. Cang J, Savier E, Barchini J, and Liu X (2018). Visual Function, Organization, and Development of the Mouse Superior Colliculus. Annu Rev Vis Sci 4, 239–262. [PubMed: 29852095]

8. Oliveira AF, and Yonehara K (2018). The Mouse Superior Colliculus as a Model System for Investigating Cell Type-Based Mechanisms of Visual Motor Transformation. Front. Neural Circuits 12, 59. [PubMed: 30140205]
9. Basso MA, and May PJ (2017). Circuits for Action and Cognition: A View from the Superior Colliculus. Annu Rev Vis Sci 3, 197–226. [PubMed: 28617660]
10. Ramón y, Cajal S Translated by Swanson N (1995). The superior colliculus In: Histology of the Nervous System New York: Oxford Univ. Press, ed. (New York: Oxford Univ. Press).
11. Gale SD, and Murphy GJ (2014). Distinct representation and distribution of visual information by specific cell types in mouse superficial superior colliculus. J. Neurosci 34, 13458–13471. [PubMed: 25274823]
12. Hoy JL, Yavorska I, Wehr M, and Niell CM (2016). Vision Drives Accurate Approach Behavior during Prey Capture in Laboratory Mice. Curr. Biol 26, 3046–3052. [PubMed: 27773567]
13. Shang C, Liu A, Li D, Xie Z, Chen Z, Huang M, Li Y, Wang Y, Shen WL, and Cao P (2019). A subcortical excitatory circuit for sensory-triggered predatory hunting in mice. Nat. Neurosci 22, 909–920. [PubMed: 31127260]
14. Shang C, Liu Z, Chen Z, Shi Y, Wang Q, Liu S, Li D, and Cao P (2015). A parvalbumin-positive excitatory visual pathway to trigger fear responses in mice. Science 348, 1472–1477. [PubMed: 26113723]
15. Wei P, Liu N, Zhang Z, Liu X, Tang Y, He X, Wu B, Zhou Z, Liu Y, Li J, et al. (2015). Processing of visually evoked innate fear by a non-canonical thalamic pathway. Nat. Commun 6, 6756. [PubMed: 25854147]
16. Shang C, Chen Z, Liu A, Li Y, Zhang J, Qu B, Yan F, Zhang Y, Liu W, Liu Z, et al. (2018). Divergent midbrain circuits orchestrate escape and freezing responses to looming stimuli in mice. Nat. Commun 9, 1232. [PubMed: 29581428]
17. Zhu H, and Roth BL (2014). Silencing Synapses with DREADDs. Neuron 82, 723–725. [PubMed: 24853931]
18. Gerfen CR, Paletzki R, and Heintz N (2013). GENSAT BAC Cre-Recombinase Driver Lines to Study the Functional Organization of Cerebral Cortical and Basal Ganglia Circuits. Neuron 80, 1368–1383. [PubMed: 24360541]
19. Villalobos CA, Wu Q, Lee PH, May PJ, and Basso MA (2018). Parvalbumin and GABA Microcircuits in the Mouse Superior Colliculus. Front. Neural Circuits 12, 35. [PubMed: 29780307]
20. Lima SQ, Hromádka T, Znamenskiy P, and Zador AM (2009). PINP: a new method of tagging neuronal populations for identification during in vivo electrophysiological recording. PLoS One 4, e6099. [PubMed: 19584920]
21. Madisen L, Mao T, Koch H, Zhuo J-M, Berenyi A, Fujisawa S, Hsu Y-WA, Garcia AJ 3rd, Gu X, Zanella S, et al. (2012). A toolbox of Cre-dependent optogenetic transgenic mice for light-induced activation and silencing. Nat. Neurosci 15, 793–802. [PubMed: 22446880]
22. Stachniak TJ, Ghosh A, and Sternson SM (2014). Chemogenetic synaptic silencing of neural circuits localizes a hypothalamus→midbrain pathway for feeding behavior. Neuron 82, 797–808. [PubMed: 24768300]
23. Bennett C, Gale SD, Garrett ME, Newton ML, Callaway EM, Murphy GJ, and Olsen SR (2019). Higher-Order Thalamic Circuits Channel Parallel Streams of Visual Information in Mice. Neuron. Available at: 10.1016/j.neuron.2019.02.010.
24. Piscopo DM, El-Danaf RN, Huberman AD, and Niell CM (2013). Diverse visual features encoded in mouse lateral geniculate nucleus. J. Neurosci 33, 4642–4656. [PubMed: 23486939]
25. Niell CM, and Stryker MP (2008). Highly selective receptive fields in mouse visual cortex. J. Neurosci 28, 7520–7536. [PubMed: 18650330]
26. Chen SC, Morley JW, and Solomon SG (2015). Spatial precision of population activity in primate area MT. Journal of Neurophysiology 114, 869–878. Available at: 10.1152/jn.00152.2015. [PubMed: 26041825]
27. Roth MM, Dahmen JC, Muir DR, Imhof F, Martini FJ, and Hofer SB (2016). Thalamic nuclei convey diverse contextual information to layer 1 of visual cortex. Nat. Neurosci 19, 299–307. [PubMed: 26691828]

28. Beltramo R, and Scanziani M (2019). A collicular visual cortex: Neocortical space for an ancient midbrain visual structure. Science 363, 64–69. [PubMed: 30606842]
29. Doubell TP, Skaliora I, Baron J, and King AJ (2003). Functional connectivity between the superficial and deeper layers of the superior colliculus: an anatomical substrate for sensorimotor integration. J. Neurosci 23, 6596–6607. [PubMed: 12878701]
30. Schiller PH, and Stryker M (1972). Single-unit recording and stimulation in superior colliculus of the alert rhesus monkey. J. Neurophysiol 35, 915–924. [PubMed: 4631839]
31. Mohler CW, and Wurtz RH (1976). Organization of monkey superior colliculus: intermediate layer cells discharging before eye movements. J. Neurophysiol 39, 722–744. [PubMed: 823302]
32. Mysore SP, and Knudsen EI (2013). A shared inhibitory circuit for both exogenous and endogenous control of stimulus selection. Nat. Neurosci 16, 473–478. [PubMed: 23475112]
33. Asadollahi A, and Knudsen EI (2016). Spatially precise visual gain control mediated by a cholinergic circuit in the midbrain attention network. Nat. Commun 7, 13472. [PubMed: 27853140]
34. Cruz-Martín A, El-Danaf RN, Osakada F, Sriram B, Dhande OS, Nguyen PL, Callaway EM, Ghosh A, and Huberman AD (2014). A dedicated circuit links direction-selective retinal ganglion cells to the primary visual cortex. Nature 507, 358–361. [PubMed: 24572358]
35. Bickford ME, Zhou N, Krahe TE, Govindaiah G, and Guido W (2015). Retinal and Tectal "Driver-Like" Inputs Converge in the Shell of the Mouse Dorsal Lateral Geniculate Nucleus. J. Neurosci 35, 10523–10534. [PubMed: 26203147]
36. Zhao Z-D, Chen Z, Xiang X, Hu M, Xie H, Jia X, Cai F, Cui Y, Chen Z, Qian L, et al. (2019). Zona incerta GABAergic neurons integrate prey-related sensory signals and induce an appetitive drive to promote hunting. Nat. Neurosci 22, 921–932. [PubMed: 31127258]
37. Han W, Tellez LA, Rangel MJ Jr, Motta SC, Zhang X, Perez IO, Canteras NS, Shammah-Lagnado SJ, van den Pol AN, and de Araujo IE (2017). Integrated Control of Predatory Hunting by the Central Nucleus of the Amygdala. Cell 168, 311–324.e18. [PubMed: 28086095]
38. Li Y, Zeng J, Zhang J, Yue C, Zhong W, Liu Z, Feng Q, and Luo M (2018). Hypothalamic Circuits for Predation and Evasion. Neuron 97, 911–924.e5. [PubMed: 29398361]
39. Park S-G, Jeong Y-C, Kim D-G, Lee M-H, Shin A, Park G, Ryoo J, Hong J, Bae S, Kim C-H, et al. (2018). Medial preoptic circuit induces hunting-like actions to target objects and prey. Nat. Neurosci 21, 364–372. [PubMed: 29379117]
40. Drager UC, and Hubel DH (1975). Physiology of visual cells in mouse superior colliculus and correlation with somatosensory and auditory input. Nature 253, 203–204. [PubMed: 1110771]
41. Zhao X, Liu M, and Cang J (2014). Visual Cortex Modulates the Magnitude but Not the Selectivity of Looming-Evoked Responses in the Superior Colliculus of Awake Mice. Neuron 84, 202–213. Available at: 10.1016/j.neuron.2014.08.037. [PubMed: 25220812]
42. Liang F, Xiong XR, Zingg B, Ji X-Y, Zhang LI, and Tao HW (2015). Sensory Cortical Control of a Visually Induced Arrest Behavior via Corticotectal Projections. Neuron 86, 755–767. [PubMed: 25913860]
43. Zingg B, Chou X-L, Zhang Z-G, Mesik L, Liang F, Tao HW, and Zhang LI (2017). AAV-Mediated Anterograde Transsynaptic Tagging: Mapping Corticocollicular Input-Defined Neural Pathways for Defense Behaviors. Neuron 93, 33–47. [PubMed: 27989459]
44. Wang L, and Krauzlis RJ (2018). Visual Selective Attention in Mice. Curr. Biol 28, 676–685.e4. [PubMed: 29456140]
45. Hippenmeyer S, Vrieseling E, Sigrist M, Portmann T, Laengle C, Ladle DR, and Arber S (2005). A developmental switch in the response of DRG neurons to ETS transcription factor signaling. PLoS Biol. 3, e159. [PubMed: 15836427]
46. Krashes MJ, Koda S, Ye C, Rogan SC, Adams AC, Cusher DS, Maratos-Flier E, Roth BL, and Lowell BB (2011). Rapid, reversible activation of AgRP neurons drives feeding behavior in mice. J. Clin. Invest 121, 1424–1428. [PubMed: 21364278]
47. Paxinos G, and Franklin KBJ (2012). Paxinos and Franklin's the Mouse Brain in Stereotaxic Coordinates (Academic Press).

48. Comoli E, Das Neves Favaro P, Vautrelle N, Leriche M, Overton PG, and Redgrave P (2012). Segregated anatomical input to sub-regions of the rodent superior colliculus associated with approach and defense. Front. Neuroanat 6, 9. [PubMed: 22514521]

49. Tervo DGR, Hwang B-Y, Viswanathan S, Gaj T, Lavzin M, Ritola KD, Lindo S, Michael S, Kuleshova E, Ojala D, et al. (2016). A Designer AAV Variant Permits Efficient Retrograde Access to Projection Neurons. Neuron 92, 372–382. [PubMed: 27720486]

50. Hoy JL, and Niell CM (2015). Layer-specific development of receptive field properties and network synchrony in mouse visual cortex. Int. J. Dev. Neurosci 47, 130.

51. Niell CM, and Stryker MP (2010). Modulation of visual responses by behavioral state in mouse visual cortex. Neuron 65, 472–479. [PubMed: 20188652]

52. Dombeck DA, Khabbaz AN, Collman F, Adelman TL, and Tank DW (2007). Imaging Large-Scale Neural Activity with Cellular Resolution in Awake, Mobile Mice. Neuron 56, 43–57. [PubMed: 17920014]

53. Roux L, Stark E, Sjulson L, and Buzsáki G (2014). In vivo optogenetic identification and manipulation of GABAergic interneuron subtypes. Curr. Opin. Neurobiol 26, 88–95. [PubMed: 24440414]

54. Kravitz AV, Owen SF, and Kreitzer AC (2013). Optogenetic identification of striatal projection neuron subtypes during in vivo recordings. Brain Res. 1511, 21–32. [PubMed: 23178332]

55. Brainard DH (1997). The Psychophysics Toolbox. Spat. Vis 10, 433–436. [PubMed: 9176952]

56. Pelli DG (1997). The VideoToolbox software for visual psychophysics: transforming numbers into movies. Spat. Vis 10, 437–442. [PubMed: 9176953]

57. Harris KD, Henze DA, Csicsvari J, Hirase H, and Buzsáki G (2000). Accuracy of Tetrode Spike Separation as Determined by Simultaneous Intracellular and Extracellular Measurements. J. Neurophysiol 84, 401–414. [PubMed: 10899214]

58. Schneider CA, Rasband WS, Eliceiri KW (2012). NIH Image to ImageJ: 25 years of image analysis. Nature Methods. 9, 671–675. [PubMed: 22930834]

Highlights

- Cell types in the superior colliculus differentially contribute to prey capture
- Wide-field vertical neurons are required for prey detection and approach initiation
- Narrow-field vertical neurons are required for accurate and continuous approaches
- Connectivity and visual responses are consistent with the role in behavior

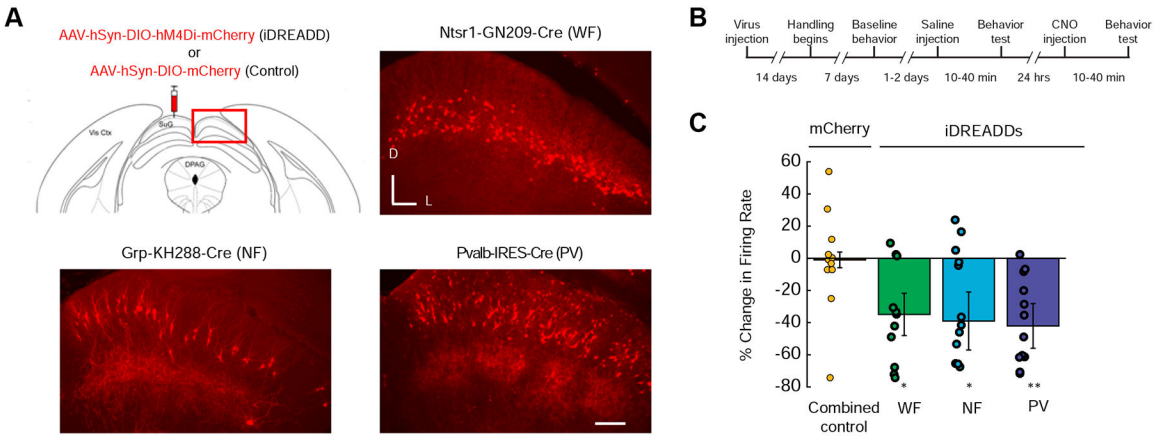

Figure 1. DREADD-mediated inhibition of three different cell types in mouse superior colliculus.

(A) Top left: AAV virus delivering either hM4Di fused to mCherry (iDREADDs) or mCherry only (control) was injected bilaterally into sSC, as shown in coronal section centered on the injection site (adapted from Paxinos 2004). The red box outlines the area of sSC shown in the top right and bottom panels from each Cre line injected. Top right and bottom panels: Fluorescence expression pattern following iDREADD + mCherry AAV injection into three separate Cre-lines. Scale bar 100 μm, D/L = Dorsal/Lateral. WF = widefield neurons, NF = narrowfield neurons, PV = parvalbumin-positive neurons. (B) Timeline of experimental manipulation and behavioral assessment of each of the treatment groups. (C) Median percent change in average ring rate during stimulus presentation from before to 10 min after CNO injection, for neurons from all treatment groups. The combined control is the result from all mice expressing mCherry-only in each of the three cell types. Control = 11 cells, 9 mice; WF = 11 cells, 5 mice; NF = 12 cells, 6 mice; PV = 12 cells, 7 mice. Significance tested using Wilcoxon signed rank test, testing for a median equal to 0, **= $p<0.01$, *=$p<0.05$. Error bars are +/− standard error of the median. See also Figure S1.

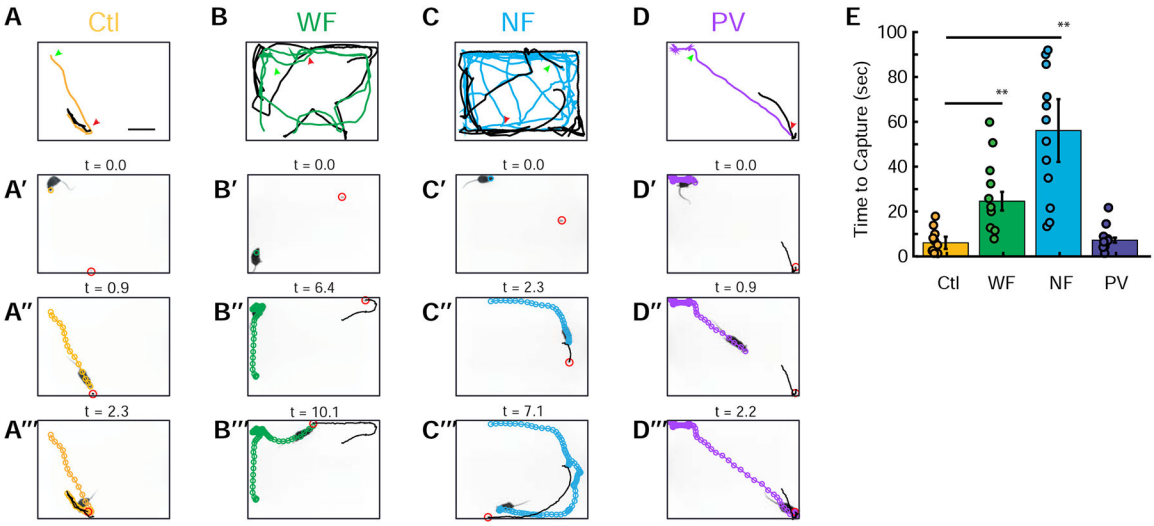

Figure 2. Inhibition of WF and NF cells distinctly perturbs prey capture behavior.

(A-D) Top row: representative tracks from a single trial (total duration through final capture) from each experimental group, following CNO injection. Arrows indicate the start point (green) and end point (red) of an individual approach sequence within the trial. Scale bar 10 cm. Bottom rows: representative detection and approach sequence (extracted from the trial in top row and labeled with arrows) following inhibition of cell types. (A'-A") Control mCherry-only, see also Video S1. (B'-B"') WF cells suppressed, see also Video S2. (C'-C"') NF cells suppressed, see also Video S3 (D'-D"') PV cells suppressed, see also Video S4. Note the difference in total time for each approach sequence as compared to control. Colored circle tracks denote head position marked at 16 ms intervals. Red circles highlight cricket location. (E) Median cricket capture time for each group. n=10, 10, 12, 9 mice in control, WF, NF, PV respectively. Significance tested for by Mann-Whitney U. **=$p<0.01$. Error bars are +/− standard error of the median. See also Figure S2 and Videos S1–S4.

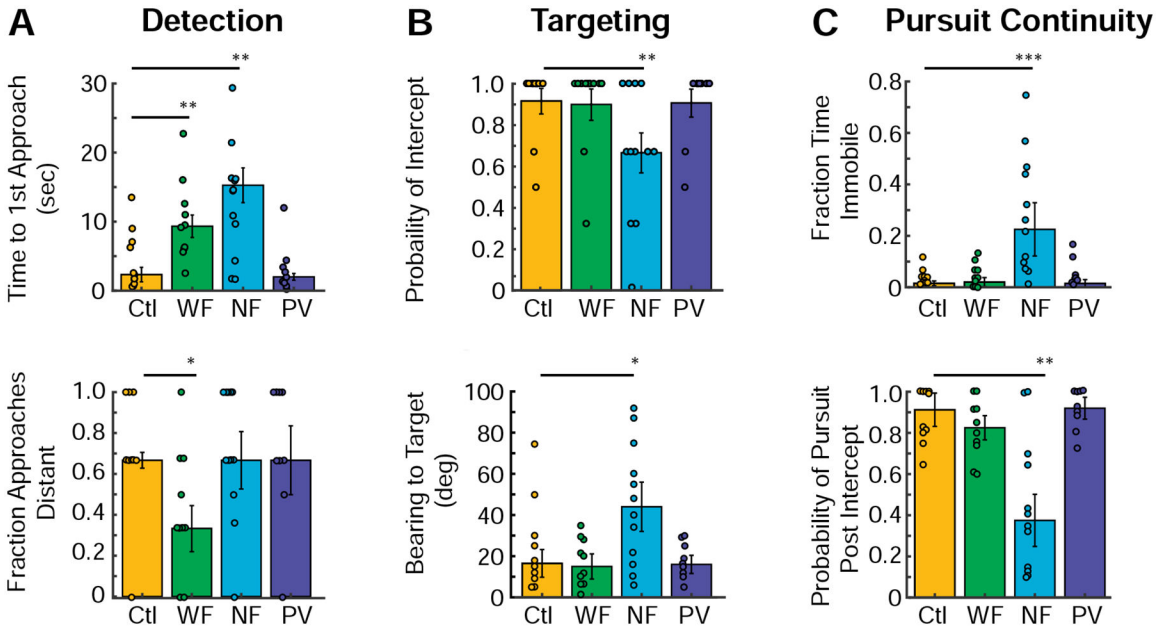

Figure 3. Suppression of specific cell types differentially alters target detection and pursuit behavior

(A) Detection performance. Top: Median time to first approach. Bottom: Mean fraction of distant approaches (greater than15 cm from target) per mouse. (B) Targeting performance. Top: Probability of an intercept following initiation of first approach. Bottom: Median bearing to target when the mouse is within 5 cm during an approach that ends in contact. (C) Pursuit continuity. Top: Median percent time immobile within 5 cm of the prey. Bottom: Probability mouse will successfully re-initiate pursuit in < 1 second following interception if it fails to capture. All data points are trial-averaged data, 2–3 trials per mouse. Significance tested using Kruskal-Wallis, α=0.05, followed by Mann-Whitney-U and Dunn-Sidak correction for multiple comparisons. n=10, 10, 12, 9, control, WF, NF and PV mice respectively. ***=p<0.001, **=p<0.01, *=p<0.05. Error bars are standard error of the median where medians are shown. Error bars are ± SEM for means. See also Figure S3 and Videos S1–S4.

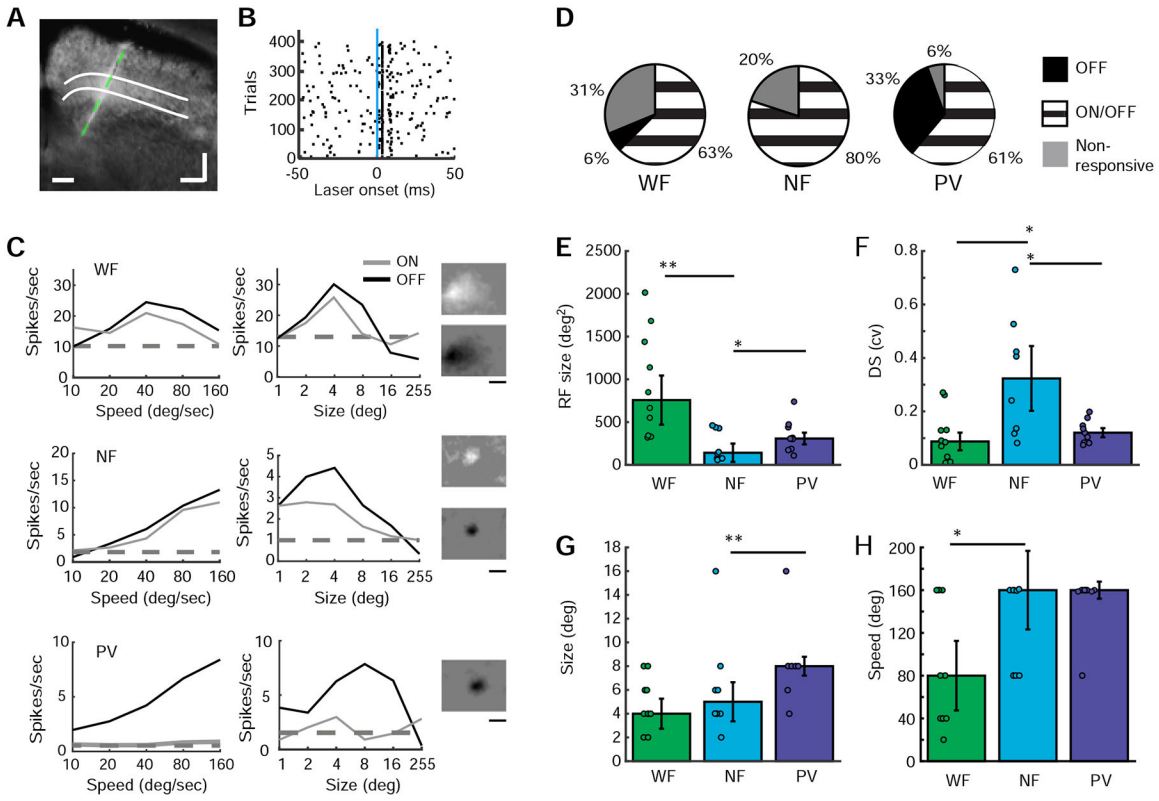

Figure 4. Visual response properties of WF, NF and PV cells in the awake mouse.

(A) Representative image of an electrode track recovered following recording in an Ntsr1-GN209-Cre mouse expressing Cre-dependent ChR2 in WF neurons. Scale bar equals 100 μm, D=dorsal and M=medial, parallel white bars demarcate stratum opticum (SO). (B) Identification of Cre+/ChR2+ neurons based on response to optogenetic light stimulation. ChR2+ neurons (Cre+) demonstrated short-latency responses (<1.5 ms) with little jitter (<1.5 ms) to blue light stimulation as shown by spike rasters for repeated trials. Blue line indicates laser onset time (1 ms duration). (C) Representative speed and size tuning curves from a WF neuron (top row), NF neuron (middle row), PV neuron (bottom row). Insets show representative spike triggered averages of the responses to sparse, moving ON (top) and OFF (bottom) spots, respectively. Scale bar equals 20 deg. (D) Categorization of response types based on flashing spot stimuli, n=27, 16, and 23, WF, NF, and PV cells from 10, 8 and 9 animals, respectively. (E) Median estimated receptive field size based on spike triggered averages of either ON or OFF response to moving spot stimuli, for cells that were well-fit by a Gaussian function and (F) Median direction selectivity, based on circular variance, by cell type. Responses per animal were averaged, n=10, 8, and 9, in WF, NF, and PV animals, respectively. (G) Median preferred size for selective units averaged per animal, n= 9, 8, and 7, WF, NF, and PV animals, respectively. In three animals, no size selective responses were observed. (H) Median preferred speed for selective units averaged per animal, n=9, 7, and 7, WF, NF, and PV animals, respectively. In four animals, no speed selective responses were observed. Significance tested using Kruskal-Wallis, α =0.05, followed by Mann-Whitney-U

and Dunn-Sidak correction for multiple comparisons. **=p<0.01, *=p<0.05. Error bars are standard error of the median.

KEY RESOURCES TABLE

REAGENT or RESOURCE	SOURCE	IDENTIFIER
Antibodies		
Bacterial and Virus Strains		
AAV8-hSyn-DIO-hM4D(Gi)-mCherry	viral particles from Addgene- Dr. Bryan Roth	44362-AAV8
AAV8-hSyn-DIO-mCherry	viral particles from Addgene - Dr. Bryan Roth	44362-AAV8
Biological Samples		
Chemicals, Peptides, and Recombinant Proteins		
Clozapine-N-Oxide	Enzo	BML-NS105-0005
Critical Commercial Assays		
Deposited Data		
Experimental Models: Cell Lines		
Experimental Models: Organisms/Strains		
Mice: Ntsr1–GN209–Cre (B6;129S6)	Dr.s Charles Gerfen and Nathanial Heintz	
Mice: Grp-KH288-Cre (B6;129S6)	Dr.s Charles Gerfen and Nathanial Heintz	
Pvalb-IRES-Cre- B6;129P2	The Jackson Laboratory	JAX stock #008069
Ai32(RCL-ChR2(H134R)/EYFP)-C57BL/6J congenic	The Jackson Laboratory	JAX stock #012569
Oligonucleotides		
Recombinant DNA		
Software and Algorithms		
Custom Matlab scripts	Mathworks	
Psychophysics Toolbox	Dr. David Brainard	
Psychophysics Toolbox extension	Dr. Denis Pelli	
ImageJ	[58]	https://imagej.nih.gov/ij/
Other		
RZ2 BioAmp Processor and PZ2 amplifier	Tucker Davis Technologies	System 3 workstation
32 site, linear electrodes with 50 mM diameter optic fiber	Neuronexus Technologies	A1×32-5mm-25-177-OA32LP